



UNIVERSITY OF LEEDS

This is a repository copy of *A natural, cellulose-based microgel for water-in-oil emulsions*.

White Rose Research Online URL for this paper:

<https://eprints.whiterose.ac.uk/167781/>

Version: Accepted Version

---

**Article:**

Lefroy, KS, Murray, BS [orcid.org/0000-0002-6493-1547](https://orcid.org/0000-0002-6493-1547), Ries, ME [orcid.org/0000-0002-8050-3200](https://orcid.org/0000-0002-8050-3200) et al. (1 more author) (2021) A natural, cellulose-based microgel for water-in-oil emulsions. *Food Hydrocolloids*, 113. 106408. ISSN 0268-005X

<https://doi.org/10.1016/j.foodhyd.2020.106408>

---

© 2020, Elsevier Ltd. This manuscript version is made available under the CC-BY-NC-ND 4.0 license <http://creativecommons.org/licenses/by-nc-nd/4.0/>.

**Reuse**

This article is distributed under the terms of the Creative Commons Attribution-NonCommercial-NoDerivs (CC BY-NC-ND) licence. This licence only allows you to download this work and share it with others as long as you credit the authors, but you can't change the article in any way or use it commercially. More information and the full terms of the licence here: <https://creativecommons.org/licenses/>

**Takedown**

If you consider content in White Rose Research Online to be in breach of UK law, please notify us by emailing [eprints@whiterose.ac.uk](mailto:eprints@whiterose.ac.uk) including the URL of the record and the reason for the withdrawal request.



[eprints@whiterose.ac.uk](mailto:eprints@whiterose.ac.uk)  
<https://eprints.whiterose.ac.uk/>

# A Natural, Cellulose-Based Microgel for Water-in-Oil Emulsions

Katherine S. Lefroy<sup>1</sup>, Brent S. Murray<sup>1\*</sup>, Michael E. Ries<sup>2</sup>, Thomas D. Curwen<sup>3</sup>

<sup>1</sup>Food Colloids & Bioprocessing Group, School of Food Science & Nutrition, University of Leeds, UK

<sup>2</sup>Soft Matter Physics Group, School of Physics & Astronomy, University of Leeds, UK

<sup>3</sup>Mondelēz International, Reading Science Centre, UK

\* Author for correspondence

b.s.murray@leeds.ac.uk

**Declarations of interest:** none

18 **Abstract**

19

20 Non-derivatised cellulose is generally assumed to have poor surface activity and  
21 therefore be unsuitable as a water in oil (W/O) emulsifier. In this work, a “natural”  
22 cellulose microgel (CMG) is fabricated via a top-down approach and used to stabilise  
23 W/O emulsions, without employing chemical modification. The cellulose is  
24 coagulated from an ionic liquid through a solvent-exchange process, in the presence  
25 and absence of added sunflower oil, in order to tune the cellulose morphology and  
26 properties. Detailed characterization of the nature of these microgels and the effect  
27 of the solvent change sequence on their emulsifying properties was investigated. In  
28 the presence of oil, Fourier transform infrared (FTIR) spectroscopy confirmed the  
29 retention of oil in the coagulum during regeneration and the resultant CMGs were  
30 more easily dispersed in oil than water, suggesting the fabrication of a “hydrophobic”  
31 microgel. Confocal microscopy confirmed the adsorption of CMGs to the water-oil  
32 interface and W/O emulsions of up to 20 vol.% water displayed good stability over at  
33 least 1 month. This study therefore describes a “novel” route to W/O stabilisation  
34 using a natural emulsifier, which could be then used as a method of reducing fat and  
35 sugar in food products.

36

37 **Keywords:** cellulose; microgel; W/O; emulsion; ionic liquid; anti-solvent

38

39

40  
41  
42  
43  
44  
45  
46  
47  
48  
49  
50  
51  
52  
53  
54  
55  
56  
57  
58  
59  
60  
61  
62  
63  
64  
65  
66  
67  
68  
69  
70  
71  
72  
73  
74  
75  
76  
77  
78  
79  
80  
81  
82  
83  
84  
85  
86  
87  
88  
89

## 1. Introduction

The dramatic rise in obesity levels over the last few decades has been linked to the increased availability of high-energy foods, as well as genetic susceptibility and reduced physical activity (Kopelman, 2000). Reducing the calories in food products is not only demanded by consumers but is also an effective method for lessening the impact of obesity and related health problems (Borreani, Hernando, & Quiles, 2020). The World Health Organization (WHO) recommends reformulation of foods in order to reduce *trans*-fat, fat and free-sugar content, with the goal of eventually eliminating *trans*-fats completely (Rogers, Wright, & Marangoni, 2009).

High-calorie confectionary products such as creams, fillings and spreads are “rich” in texture and taste and highly desired by consumers for the feelings of luxury and indulgency they impart, but reducing the fat content without affecting product quality is a huge challenge (Borreani et al., 2020). Within the food industry, water is an attractive replacement for fat and sugar. Forming a water-in-oil (W/O) emulsion and thus reducing the overall fat content, as opposed to using a bulking agent, allows the ‘smoothness’ and ‘creaminess’ of products to be maintained (Marchetti, Muzzio, Cerrutti, Andrés, & Califano, 2017; Mitsou et al., 2016). Furthermore, it has been shown that perceived ‘creaminess’ is directly correlated to emulsion viscosity and therefore controlling bulk rheological properties of a system allows manipulation of its sensory attributes, regardless of droplet size and water-volume fraction (Dickinson, 2011).

W/O emulsions are already used extensively in the food, pharmaceutical, agricultural and cosmetic industries in order to deliver and protect functional compounds, modify sensory properties and improve shelf-life, amongst other things (Albert et al., 2019; Azmi, Elgharbawy, Motlagh, Samsudin, & Salleh, 2019; Martinez, Rosado, Velasco, Lannes, & Baby, 2019; McClements, 2004; Neethirajan et al., 2011). The usual way of preparation is to disperse a hydrophobic emulsifier in the oil phase, followed by addition of water under mechanical agitation to yield an emulsion of stabilised water droplets.

Since for W/O emulsions the emulsifier must be dispersible in the continuous oil phase, generally non-ionic, (i.e. uncharged) low hydrophilic-lipophilic balance (HLB) surfactants are utilized, so that steric stabilization might be thought to be the dominant mechanism (Bastida-Rodríguez, 2013). However, charges and dipoles may still be present at the interface, that result in significant long-range electrostatic repulsion between droplets across the low dielectric constant oil phase. This is still likely with particulate stabilizers, i.e. Pickering emulsions, where hydrophobic particles may still carry a range of ionizable groups or adsorbed or trapped ionic species. Particles ranging in size from a few 10s of nm to several  $\mu\text{m}$  have proved effective as Pickering emulsifiers. Unlike surfactants, true Pickering stabilizers are insoluble in both oil and water, and are characterised by their wettability or contact angle (Murray, 2019b; Wang & Wang, 2016). Particles have numerous advantages over more traditional surfactants used in foods, for example the superior stability against coalescence they impart at much lower concentrations, due to their extremely high affinity for the interface (high energy of desorption) and the large steric barrier they give due to their size (Dickinson, 2012; Ghosh & Rousseau, 2011).

90 Ideally Pickering stabilizers of W/O emulsions should be 1  $\mu\text{m}$  or less, in order to  
91 stabilize droplets that are small enough to avoid flocculation, coalescence and/or  
92 rapid sedimentation. Microgels, or microgel particles have been shown to be very  
93 effective emulsion stabilizers, acting similarly to classic Pickering stabilizers (Murray,  
94 2019a, 2019b).

95  
96 Particles may play a very important role in future W/O formulations in foods (and  
97 other consumer products) because there is a considerable lack of acceptable W/O  
98 surfactants available to food manufacturers. To our knowledge, all of those currently  
99 approved have a limit on their usage (Murray, 2019b). For example, polyglycerol  
100 polyricinoleate (PGPR) has a maximum level of 4g/kg in dressings, spreadable fats  
101 and similar spreadable products, and of 5g/kg in chocolate in Europe (Bastida-  
102 Rodríguez, 2013). Whilst PGPR is considered to have no toxicity and carcinogenicity  
103 at these levels, it has been removed from certain chocolate brands due to consumer  
104 demand (Mortensen et al., 2017; Wilson & Smith, 1998) (Fox Business,  
105 [https://www.foxbusiness.com/features/hersheys-remake-of-the-great-american-  
106 chocolate-bar](https://www.foxbusiness.com/features/hersheys-remake-of-the-great-american-chocolate-bar), accessed March 2020). Furthermore, PGPR is conventionally  
107 produced via a four-stage chemical process, requiring long reaction times and high  
108 operating temperatures (Bastida-Rodríguez, 2013). The demand for alternative  
109 natural emulsifiers which involve simple, non-chemical routes to production is  
110 increasing, with emphasis on providing 'clean-label' foodstuffs (Ozturk &  
111 McClements, 2016). The use of particles in food products is therefore particularly  
112 attractive due to the lower amount of emulsifier required, the fact that they are not  
113 produced via chemical synthesis and also that they may provide reduced irritancy to  
114 the skin and membranes, since they do not have a typical 'detergent-like' structure  
115 (Arditty, Whitby, Binks, Schmitt, & Leal-Calderon, 2003).

116  
117 Much recent attention has been turned to the functionalisation of cellulose in its  
118 native form without chemical modification. Commonly found in plant cell walls,  
119 cellulose is well known for its highly robust structure which arises from a large  
120 volume of physical contacts between polysaccharide chains. Both inter- and  
121 intramolecular H-bonds form between the glucopyranose rings, reinforcing the highly  
122 repetitive crystalline structure. Within the food industry, native cellulose has also  
123 begun to emerge as a potential Pickering stabiliser, thickener and reinforcing agent  
124 for packaging, for example (Huang et al., 2020). From an ingredient perspective,  
125 cellulose is colourless, odourless and tasteless as well as an important dietary fibre.  
126 Incorporation of 'natural' cellulose into a food matrix therefore has the potential to not  
127 only significantly reduce the calorie-content, but to also improve its nutritional make-  
128 up (Gómez & Martinez, 2018).

129  
130 Large scale cellulose solubilisation is traditionally achieved using the Viscose  
131 process, which has numerous disadvantages such as complex reaction conditions,  
132 slow reaction times and harmful side products (Paunonen et al., 2019; J. Zhang et  
133 al., 2017). Such method results in grafting of groups onto the cellulose chains during  
134 dissolution, producing so-called derivatised cellulose. This charges the surface of the  
135 cellulose and affects its swelling properties as well as its ability to act as an  
136 emulsifier, since electrostatic repulsion between particles leads to a higher barrier for  
137 interfacial adsorption (Bertsch et al., 2019; Stana-Kleinschek, Ribitsch, Kreze, &  
138 Fras, 2002). Alternative non-derivatising solvent systems such as NaOH/aqueous  
139 solutions (Qi, Yang, Zhang, Liebert, & Heinze, 2011), *N,N*-dimethylacetamide

140 (DMAc)/LiCl (Sadeghifar, Venditti, Pawlak, & Jur, 2019) and ionic liquids (ILs) (J.  
141 Zhang et al., 2017) have been developed on a small scale, with the aim of producing  
142 non-grafted regenerated cellulose in an environmentally friendly manner (Cai &  
143 Zhang, 2005). In this particular work, we focus on ILs as cellulose solvents.

144  
145 Numerous ILs have been reported to dissolve large amounts of cellulose without  
146 chemical modification, under mild conditions and with possible recovery and reuse of  
147 the solvent afterwards (Verma et al., 2019). Amongst these, two of the most common  
148 solvents employed are 1-ethyl-3-methylimidazolium acetate (EmimAc) and 1-butyl-3-  
149 methylimidazolium acetate (BmimAc). More recently, ILs have been prepared from  
150 renewable raw materials and may provide even easier handling, as well as being  
151 readily bio-degradable and comparatively lower in cost (Ossowicz, Klebeko, Roman,  
152 Janus, & Rozwadowski, 2019). For example, amino-acid ILs based on cholinium  
153 have shown impressive rates of dissolution under mild conditions, even in the  
154 presence of significant amounts of water (Chua et al., 2019).

155  
156 Once dissolved in an IL, cellulose can be recovered by adding a so-called  
157 'coagulant' or 'anti-solvent,' such as water, ethanol or *n*-propanol, which is miscible  
158 with the IL but not with cellulose (Tan, Chen, Li, & Xie, 2019). Varying the  
159 coagulation conditions, as well as type and amount of anti-solvent, yields cellulose in  
160 different forms and allows manipulation of its properties (Fan et al., 2018; Gupta, Hu,  
161 & Jiang, 2013; Tan et al., 2019). Thorough washing of the regenerated cellulose also  
162 completely removes any IL, permitting recovery of the IL and anti-solvents and  
163 ensuring that the resultant cellulose is pure and safe for consumption.

164  
165 In theory, any anti-solvent which is miscible in the IL but that does not dissolve  
166 cellulose could be used as a coagulant, but thorough washing with water as a final  
167 stage is generally the most convenient way to ensure complete removal of IL, since it  
168 seems to be the most effective solvent in breaking cellulose-anion H-bonds (Gupta  
169 et al., 2013). The use of a less polar, slow-diffusing anti-solvent coagulant delays the  
170 regeneration process, allowing the gel network to form more gradually through a  
171 'softer' precipitation (Fink et al., 2001). Furthermore, 'coating' the hydrophobic planes  
172 with a non-polar molecule before regeneration could block hydrophobic interactions  
173 between cellulose chains, to a certain degree. A combination of these two  
174 approaches, firstly 'coating' and protecting hydrophobic regions in cellulose and  
175 secondly delaying reprecipitation, may increase the hydrophobicity of the  
176 regenerated cellulose. Formation of a porous gel network could not only "lock-in"  
177 such hydrophobic character, but may also allow interpenetration of phases at an  
178 interface, hereby improving its ability to function as an emulsifier (Murray, 2019b).

179  
180 In this work, BmimAc was selected as the IL for dissolution of up to 4 wt.% cellulose  
181 and the bulk macrogels generated by anti-solvent exchange were mechanically  
182 broken down to microgel particles as emulsion stabilizers, a so-called "bottom-up"  
183 approach (Murray, 2019a). To increase the hydrophobicity of the microgels an edible  
184 oil was also introduced during the anti-solvent exchange. These novel cellulose  
185 microgels were effective W/O emulsifiers – emulsions of up to 20 vol.% water were  
186 stable for at least 1 month without the addition of any other surface-active agents.  
187 This work therefore provides a potentially inexpensive, and possibly "clean label"

188 route to fat replacement in foods, using renewable resource materials and simple,  
189 convenient methodology.

190

## 191 **2. Materials and Method**

192

### 193 *2.1 Materials*

194

195 1-Butyl-3-methyl imidazolium (BmimAc) ( $\geq 95\%$  purity), ethanol (absolute, 99.8%),  
196 Calcofluor White (1 g/L), Nile red and sodium azide were obtained from Sigma  
197 Aldrich. 1-Butanol (Acros Organics, 99.5%) was obtained from Fisher Scientific.  
198 Cellulose powder (Vitacel L 600-20 and L 00) and High Oleic acid Sunflower Oil  
199 (HOSO,  $d = 0.92 \text{ g mL}^{-1}$ ) were supplied by Mondelēz International.

200

### 201 *2.2 Preparation of "non-oily" macrogel*

202 Vitacel cellulose powder (L 600-20 and L 00) was dissolved in BmimAc (1-4 wt.%)  
203 under stirring at  $75^\circ\text{C}$ , until complete dissolution (2-5h). The heated cellulose-IL  
204 solution was added dropwise through a syringe to water (2:1 v/v water/cellulose-  
205 BmimAc), with each drop forming a spherical precipitate (macrogel). The gel-water  
206 mixture was stored overnight at room temperature. Water was replaced 3 times  
207 every 4-10 h, with filtering of the macrogel in between each solvent-change (nylon  
208 membrane filter,  $0.45 \mu\text{m}$ , 45 mm). During the final filtration step, the macrogel was  
209 broken down with a spatula and washed repeatedly with deionised water to ensure  
210 complete BmimAc removal. (For example, 2 to 3 washing steps are generally able to  
211 reduce the BmimAc levels to  $< 1 \text{ ppm}$ , as detected by UV/Vis adsorption - data not  
212 shown).

### 213 *2.3 Preparation of "oily" macrogel*

214 Cellulose powder was dissolved in BmimAc as outlined in 2.2. HOSO was added  
215 directly to the heated solution (2:1 v/v HOSO/cellulose-BmimAc) and stirred using a  
216 high-speed blender (Ultra Turrax T 25, IKA, Germany) at room temperature at  
217 25,000 rpm, until complete disappearance of the phase boundary (ca. 5 mins). The  
218 HOSO-cellulose-BmimAc mixture was added dropwise through a syringe to 1-  
219 butanol (4:1 v/v 1-butanol/HOSO-cellulose-BmimAc), with each drop forming a  
220 spherical precipitate (macrogel), as on addition to water in 2.2. The gel-solvent  
221 mixture was stored overnight at room temperature. Solvent exchange and  
222 regeneration of the macrogel was conducted in the following order, using the same  
223 volumes of anti-solvent as initially added: 1-butanol, 2 x ethanol; 2 x water, with  
224 immersion in each solvent for 4-10 h. The obtained cellulose macrogel was filtered  
225 under gravity between each solvent change (nylon membrane filter,  $0.45 \mu\text{m}$ , 45  
226 mm). During the final filtration step, the macrogel was broken down and washed with  
227 deionised water, as outlined in 2.2.

228

### 229 *2.4 Preparation of cellulose microgel (CMG) dispersions in water or oil*

230

231 The non-oily and oily cellulose macrogels were dispersed in water or HOSO  
232 respectively, giving non-oily cellulose microgels (CMGs) and oily cellulose microgels  
233 (oil-CMGs). Initially, the macrogel was dispersed in the desired medium under high-

234 speed Ultra Turrax stirring (24,000 rpm, 5 min). The dispersions were then passed  
235 through a high-pressure homogeniser (Jet Homogeniser, University of Leeds)  
236 (BURGAUD, DICKINSON, & NELSON, 1990) at 300 bar with 3 passes, in order to  
237 obtain a finer CMG dispersion, then diluted to give various concentrations of CMG in  
238 water or HOSO (0.15 – 2.0 wt.%).

239

#### 240 *2.5 Preparation of oil-in-water (O/W) emulsions*

241

242 Non-oily microgels (CMGs) were briefly tested to see they had any ability to stabilize  
243 O/W emulsions (10 vol.%), prepared by adding pure HOSO dropwise to the CMG in  
244 water dispersions obtained via 2.2 and 2.4. Emulsification was carried out for a total  
245 of 5 minutes under high-speed Ultra Turrax stirring, as follows: agitation of the water  
246 phase (1 min), addition of the HOSO (2 min) and stirring of the formed emulsion (2  
247 min, all at 25,000 rpm, room temperature). The resulting emulsion was passed  
248 through the Jet Homogeniser (300 bar, 3-5 passes) and subjected to a final period of  
249 high-speed Ultra Turrax stirring (25,000 rpm, 1 min) to ensure that the two phases  
250 were fully emulsified. Sodium azide was added to all of the emulsions to prevent  
251 degradation during storage (0.05 wt.%).

252

#### 253 *2.6 Preparation of water-in-oil (W/O) emulsions*

254

255 W/O emulsions (5 to 20 vol.% water) were prepared from the dispersions of oil-CMG  
256 in HOSO or oil-CMG dispersed in water. For the former, deionised water was added  
257 dropwise to the oil-CMG dispersion in HOSO; for the latter the oil-CMG in water  
258 dispersions were added dropwise to pure HOSO. In both cases, emulsification was  
259 carried out in a total of 5 minutes under high-speed Ultra Turrax stirring, as follows:  
260 agitation of the oil phase (1 min), addition of the deionised water/oil-CMG-water  
261 dispersion (2 min) and stirring of the formed emulsion (2 min, all at 25,000 rpm, room  
262 temperature). The resulting emulsion was passed through the Jet Homogeniser (300  
263 bar 3-5 passes) and subjected to a final period of high-speed Ultra Turrax stirring  
264 (25,000 rpm, 1 min), as in 2.5. Sodium azide was added to all of the emulsions to  
265 prevent degradation during storage (0.05 wt.%).

266

267 All emulsions in 2.5 and 2.6 are described in wt.% cellulose relative to the amount of  
268 water in the system and emulsions were prepared in terms of their volume ratio,  
269 rather than weight ratio. For example, a 10 vol.% W/O emulsion stabilised by “0.2  
270 wt.% cellulose” would contain 0.2 g cellulose, 10 g (= 10 mL) of water and 83 g (= 90  
271 mL) of HOSO since the density of HOSO = 0.92 g mL<sup>-1</sup>.

272

#### 273 *2.7 Characterization of dispersions and emulsions*

274

275 The particle size distribution (PSD) of the CMG dispersions and emulsions were  
276 characterized via a Malvern Mastersizer 3000. The refractive indices of water,  
277 cellulose and HOSO were taken as 1.33, 1.47 and 1.46 respectively, and PSDs were

278 calculated based on the Mie theory. Five measurements were taken for each sample  
 279 and the average of these reported. The mean distribution of particle sizes are  
 280 displayed in terms of the surface-weighted mean diameter ( $d_{3,2}$ ), as described:  
 281

$$(d_{3,2}) = \frac{\sum_i n_i d_i^3}{\sum_i n_i d_i^2} \quad (1)$$

282 and the volume-weighted mean diameter ( $d_{4,3}$ ), as described:  
 283

$$(d_{4,3}) = \frac{\sum_i n_i d_i^4}{\sum_i n_i d_i^3} \quad (2)$$

284 where  $n_i$  gives the number of droplets;  $d_i$  gives the diameter of the particle.  
 285

286

## 287 *2.8 Attenuated Total Reflection Fourier Transform Infrared (ATR-FTIR) spectroscopy*

288

289 An Agilent 4500 series FTIR spectrometer equipped with a single reflection  
 290 attenuated total reflectance (ATR) accessory was used to analyse the changes in the  
 291 cellulose during its regeneration and the final composition of regenerated macrogels.  
 292 Each spectrum was recorded over the wavenumber range 500-3500  $\text{cm}^{-1}$  with 1640  
 293 scans, and the background was re-recorded every four measurements. Samples  
 294 were placed on the ATR crystal and uniformly spread over the measurement area  
 295 with an overhead press. Each measurement was conducted three times and an  
 296 average of these is reported for each sample. The crystal was cleaned between  
 297 each sample with distilled water and ethanol.  
 298

299

## 299 *2.9 Wide-angle X-ray scattering (WAXS)*

300

301 Wide Angle X-ray scattering (WAXS) was conducted on a SAXSpace instrument  
 302 (Anton Paar GmbH, Graz, Austria) equipped with a sealed-tube Cu-anode operating  
 303 at 40 kV and 50 mA. Cellulose powder was measured in a thin glass capillary tube,  
 304 whilst regenerated cellulose macrogels were freeze-dried and then pressed between  
 305 scattering paper into a capillary cell, to a pellet of approximately 1 mm thickness. In  
 306 all cases, the background was subtracted using the SAXSQuant software and the  
 307 scattering intensity at  $q = 0$  was set to unity, to obtain the scattered intensity,  $I(q)$ :  
 308

$$q = \frac{4\pi}{\lambda} \sin \frac{\theta}{2} \quad (3)$$

309

310 Where  $\theta$  = scattering angle and  $\lambda = 0.154$  nm (X-ray wavelength). Deconvolution of  
 311 intensity plot was carried out using peak fitting on OriginPro 9.0.

312 All ATR-FTIR and WAXS analysis was carried out at room temperature.

313

## 314 *2.10 Scanning Electron Microscopy (SEM)*

315

316 Scanning Electron Microscopy (SEM) of the cellulose macrogels was carried out  
 317 using a FEI NanoSEM Nova 450 operating at 3 kV, with a working distance of 5 mm  
 318 and an Everhart-Thornley detector (ETD). All gels were freeze-dried either straight  
 319 after water washing or after washing three times with hexane, in order to remove  
 320 excess oil from the regeneration. Freeze-dried samples were then mounted on an  
 321 SEM stub with adhesive copper tape and sputter-coated (CRESSINGTON 208 HR)  
 322 with a 2 nm iridium conductive layer.

323

### 324 *2.11 Optical microscopy and Confocal Laser Scanning microscopy (CLSM)*

325

326 The microstructure of both CMG dispersions and W/O emulsions were imaged using  
 327 a light microscope (Nikon, SMZ-2T, Japan) equipped with a digital camera (Leica  
 328 MC120 HD). Images were processed using the image analysis software ImageJ.  
 329 Confocal laser scanning microscopy (CLSM) was carried out using a Zeiss LSM700  
 330 inverted microscope (Germany) with a 20 x /0.5 objective lens. Approximately 80  $\mu\text{L}$   
 331 of sample was added to a well slide and a coverslip was placed on top (0.16-0.19  
 332 mm thickness), ensuring that no air bubbles were trapped between the sample and  
 333 coverslip. Calcofluor White was used to stain cellulose, which was added to the  
 334 sample before confocal analysis (1 g/L, 10 % v/v stain:dispersion/emulsion). Nile red  
 335 (0.4 mg mL<sup>-1</sup> in DMSO) was added to W/O emulsions in order to stain the oil phase  
 336 and analyse the shape of the water droplets (1 % v/v stain:emulsion). For Calcofluor  
 337 White, an excitation wavelength of 405 nm was used and emission between 415-470  
 338 nm measured. For Nile red, an excitation wavelength of 488 nm was used and  
 339 emission between 550-640 nm measured. Images were processed using the image  
 340 analysis software Zen.

341

### 342 *2.12 Creaming stability measurements*

343

344 3 mL of each emulsion was taken immediately after preparation and stored in a thin  
 345 tube with a sealed lid, at room temperature. Cream volume ratio was calculated by  
 346 measuring the height of the emulsion and the height of the cream using a calliper,  
 347 over a period of time, where:

$$\frac{H_2}{H_1} \times 100 = \text{Cream Volume ratio} \quad (4)$$

348 where  $H_1$  = total volume in the tube and  $H_2$  = bottom layer (water).

349

## 350 **3. Results and Discussion**

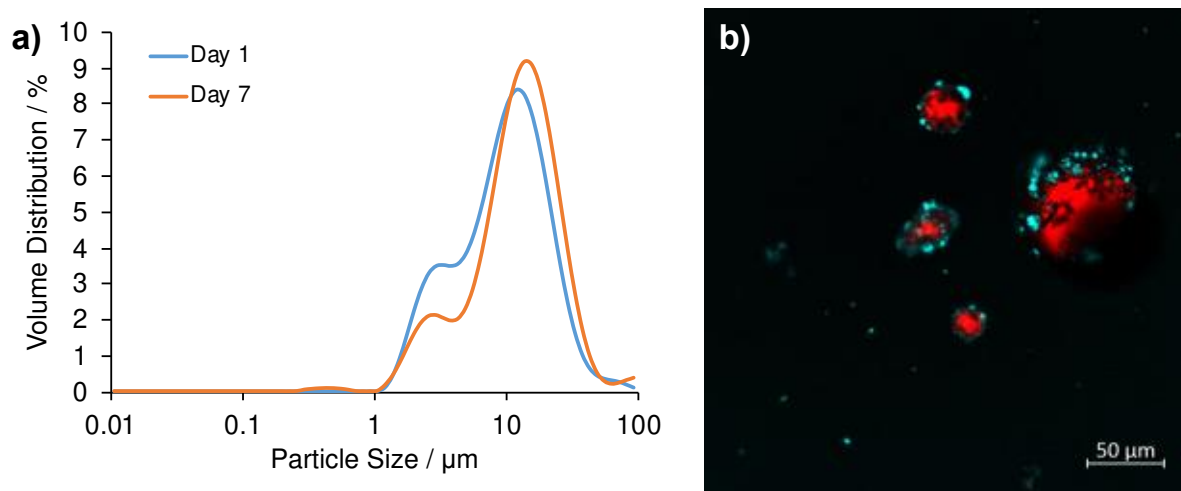
351

### 352 *3.1 Emulsions stabilised by "non-oily" CMGs (CMGs)*

353

354 Although the principal objective was to achieve W/O emulsion stabilization, the more  
 355 simple procedure of not introducing oil was tested first to see if the CMGs had any  
 356 significant surface activity at all, by testing their ability to stabilize O/W emulsions.

357 Fig. 1a gives the size distribution data over time for a 0.5 wt.% CMG-stabilised 10  
 358 vol.% O/W emulsion. A relatively monodisperse PSD was observed for all O/W  
 359 emulsions stabilised by 0.3 to 1.0 wt.% CMGs. Droplet size did not appear to change  
 360 over time and emulsions remained fairly stable to creaming (data not shown).  
 361 However, for concentrations below and above this range, flocculated droplets and  
 362 some much larger droplets were visible (Fig. A1). Furthermore, a relatively large  
 363 cream layer formed rapidly (within 5 minutes) after emulsification at CMG  
 364 concentrations greater than 0.3 wt.%, suggesting that the excess CMG does not  
 365 remain well-dispersed in the continuous phase. As seen in the confocal image (Fig.  
 366 1b), although cellulose is clearly visible at the O/W interface, surface coverage of the  
 367 oil droplets is fairly sparse. Thus, the regenerated cellulose as CMGs appeared to  
 368 display some useful hydrophobic properties and therefore surface activity, capable of  
 369 stabilizing O/W emulsions but to a limited extent. The O/W emulsions seemed to be  
 370 poorly dispersed and show tendency to aggregate in the aqueous phase with time,  
 371 particularly at higher CMG concentrations. This frustrated attempts to prepare stable  
 372 O/W emulsions with either smaller oil droplets or high volume fractions of oil  
 373 droplets. In addition, attempts to prepare W/O emulsions with CMGs were fruitless  
 374 (data not shown): at the ratios of oil to water used (section 2.6) no stable water  
 375 droplets in oil were observed. For these reasons the oil-CMG route was then largely  
 376 pursued, to try and enhance the hydrophobicity of the microgel particles, for W/O  
 377 emulsion stabilization.



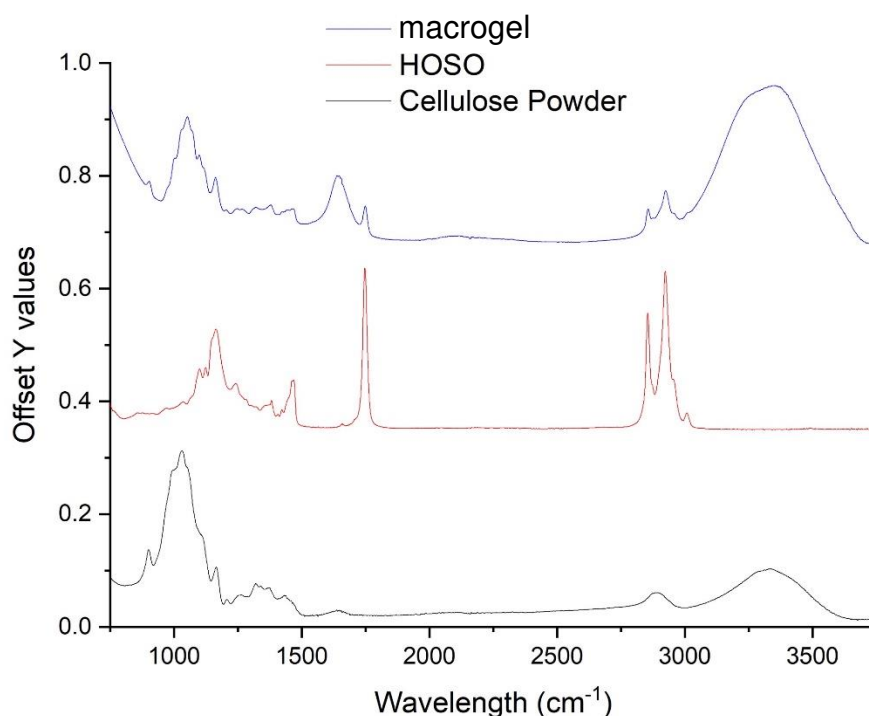
378  
 379 Fig. 1. a) PSD for 10 vol.% O/W emulsion stabilised by 0.5 wt.% CMG; b) confocal image of 10 vol.%  
 380 O/W emulsion stabilised by 1.0 wt.% CMG. Scale bar = 50 μm  
 381

### 382 3.2 Composition and structure of regenerated “oily” cellulose macrogels

383  
 384 In attempt to fabricate a CMG-based emulsifier suitable for W/O emulsions, oil was  
 385 introduced into the regeneration process (as outlined in 2.3). Fig. 2 gives the FTIR  
 386 spectra for the powdered cellulose before any treatment, pure HOSO and  
 387 regenerated macrogel. Since very similar peaks appear in both the cellulose powder  
 388 and gel, it can be said that no chemical modification of cellulose has occurred during  
 389 dissolution and regeneration (Tan et al., 2019; Xu et al., 2016). However, variation in

390 the crystal structure is apparent due to the shifting of the band at  $1433\text{ cm}^{-1}$  in the  
391 cellulose powder, which corresponds to  $\text{CH}_2$  scissoring, to a lower wavenumber  
392 ( $1425\text{ cm}^{-1}$ ) for the gel. The intensity of the peak at  $1430\text{ cm}^{-1}$  is often used to  
393 quantify the amount of cellulose I, or indeed the crystallinity of the cellulose, which in  
394 this case reduces upon regeneration. The shift in wavenumber indicates conversion  
395 from cellulose I to a different type of crystalline cellulose and/or amorphous cellulose  
396 (Fryczkowska et al., 2018; Xu et al., 2016). A band at ca.  $900\text{ cm}^{-1}$  is seen in both  
397 the powder cellulose and the gel, which can be assigned to C-O stretching in  
398 amorphous cellulose. The characteristic broad band corresponding to O-H vibrations  
399 in hydrogen bonding is observed between  $3000\text{-}3700\text{ cm}^{-1}$ , with the peak bands at  
400  $3335$  and  $3372\text{ cm}^{-1}$  for cellulose powder and gel respectively. An increase in  
401 wavenumber upon regeneration has been reported elsewhere: this shift signifies the  
402 cleavage of H-bonds between cellulose during dissolution, followed by reformation  
403 and re-structuring upon re-precipitation (Fryczkowska et al., 2018). C-O-C stretching  
404 bands (both the glucopyranose ring and glycosidic bridges) are observed in the  
405 region  $1160\text{-}1060\text{ cm}^{-1}$ . A decrease in the intensity of bands in this region for the gel  
406 is observed, most likely due to reduced order in the regenerated cellulose. Minor  
407 differences in the shape of bands are also observed, for example a shoulder is seen  
408 at  $1099\text{ cm}^{-1}$  in the gel. This indicates a difference in macromolecular structure and,  
409 more specifically, changes to the conformation of glucopyranose rings relative to  
410 adjacent cellulose chains. Therefore, a change in cellulose inter- and intramolecular  
411 H-bonding is clearly seen upon regeneration and therefore a different cellulose  
412 structure almost certainly exists in the gel.

413 Additional peaks at  $1747$ ,  $2857$  and  $2924\text{ cm}^{-1}$  are seen in the regenerated gel  
414 spectrum due to the presence of HOSO (C=O asymmetric;  $\text{CH}_3$  and  $\text{CH}_2$  stretching,  
415 (Rohman & Che Man, 2012). Peaks at  $1457$  and  $1378\text{ cm}^{-1}$  in the spectrum for pure  
416 HOSO, (corresponding to  $\text{CH}_2$  and  $\text{CH}_3$  bending respectively), are also identified in  
417 the gel. The absence of peaks at  $1384$  and  $1558\text{ cm}^{-1}$  confirms the complete removal  
418 of BmimAc during the regeneration and washing (Fig. A2). An additional intense,  
419 broad peak at  $1653\text{ cm}^{-1}$  appears, which is likely to correspond to the bending mode  
420 of water bound to cellulose (Oh, Yoo, Shin, & Seo, 2005). These observations  
421 confirm the presence of both HOSO and water in the regenerated gel, but the  
422 absence of IL.



423

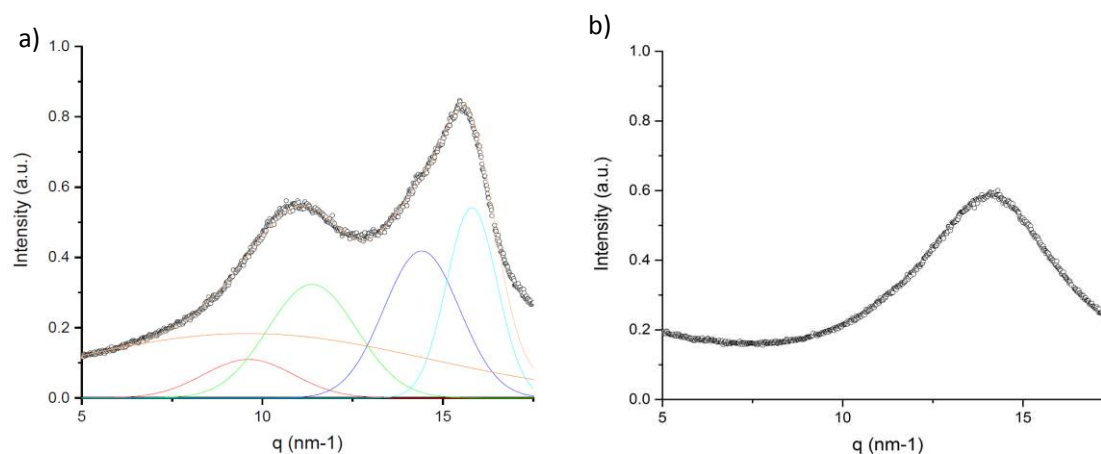
424 Fig. 2. ATR-FTIR spectra for cellulose powder (black); HOSO (red) and regenerated gel  
 425 (blue) plotted with Y offset values versus wavelength, where Y represents intensity of  
 426 absorbance (a.u.)

427 The crystal structure of the cellulose powder and regenerated macrogel were  
 428 analysed using WAXS (Fig. 3). Peaks corresponding to the (1 $\bar{1}$ 0), (110) and (200)  
 429 planes of cellulose I are known to appear at  $q \approx 10$ , 11 and 15 nm $^{-1}$  respectively, ( $2\theta \approx 14^\circ$ ,  
 430  $15^\circ$  and  $21^\circ$ ). The intensity data for the cellulose powder was deconvoluted  
 431 over this range, giving  $q \approx 9.5$ , 11.4 and 15.9 nm $^{-1}$  ( $2\theta \approx 14^\circ$ ,  $16^\circ$  and  $22^\circ$ ) along with  
 432 a broad amorphous peak and an additional peak at  $q \approx 14.3$  nm $^{-1}$  ( $2\theta \approx 20^\circ$ ) (Fig.  
 433 3a) (Fryczkowska et al., 2018; Hedlund, Köhnke, Hagman, Olsson, & Theliander,  
 434 2019; L. Sun, Chen, Jiang, & Lynch, 2015). This may be due to the presence of a  
 435 small amount of cellulose II, formed during previous processing: either scattering  
 436 from the (110) plane ( $q \approx 14.1$  nm $^{-1}$ ) or a small reflection from the (012) plane ( $q \approx$   
 437  $14.5$  nm $^{-1}$ ). However, it is more likely that peak broadening is observed simply as a  
 438 result of limited crystallite size and in this instance it can be assumed that the  
 439 cellulose powder is predominantly cellulose I (Hedlund et al., 2019).

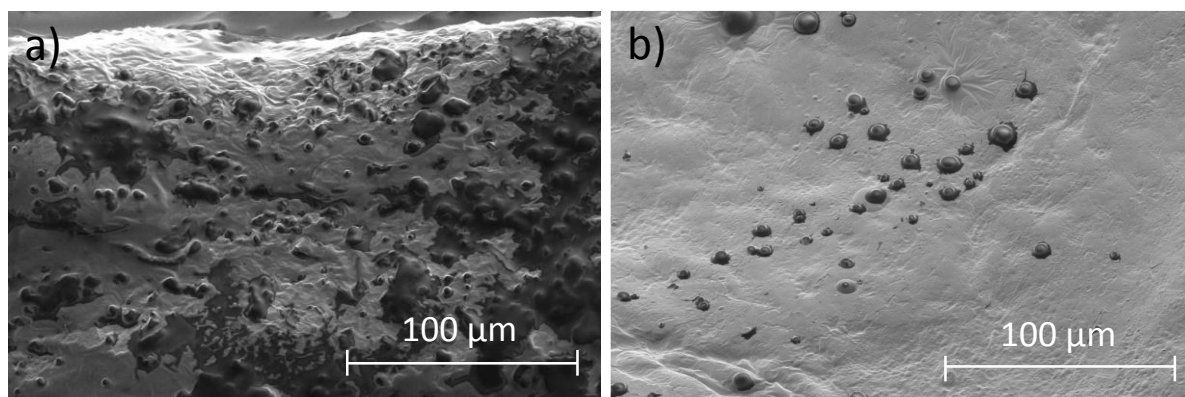
440 It is well reported that conversion from cellulose I to more thermodynamically stable  
 441 cellulose II and/or amorphous cellulose occurs during dissolution in an IL and  
 442 subsequent regeneration (Cai & Zhang, 2005; Li et al., 2018; Yan & Gao, 2008). In  
 443 particular, the use of both 1-butanol and water as coagulants has been investigated,  
 444 with both anti-solvents resulting in a reduction to crystallinity in regenerated cellulose  
 445 (Fryczkowska et al., 2018). In this instance, Fig. 3b shows the absence of long-range  
 446 order in the WAXS spectrum for the gel, due to the broadening of peaks into one  
 447 'amorphous hump.' During regeneration, fewer regular networks of cellulose intra-  
 448 and intermolecular H-bonds are able to reform and the re-packing of polysaccharide

449 chains into a crystalline form is clearly disrupted. The intensity data was not  
 450 deconvoluted to the  $(1\bar{1}0)$ ,  $(110)$  and  $(021)$  planes of cellulose II ( $q \approx 12.6$ ,  $20.3$  and  
 451  $21.2 \text{ nm}^{-1}$  respectively), since the scattering was too broad. It can be assumed that  
 452 the regenerated cellulose is mostly amorphous and any crystallinity present is of  
 453 short-range order.

454 Fig. 4 shows representative SEM images for the cellulose macrogels before and  
 455 after hexane washing (a and b respectively). It is assumed that HOSO appears as  
 456 black and cellulose as grey, in which case it is evident that a significant amount of  
 457 HOSO may remain in contact with the cellulose (although the majority is removed).  
 458 This provides some evidence for an interaction between cellulose and HOSO during  
 459 coagulation, as also seen via FTIR. Such interaction could also account for the  
 460 absence of regenerated crystalline cellulose (cellulose II) in the WAXS spectrum  
 461 (Fig. 3b), since the presence of HOSO may disrupt the re-packing of cellulose chains  
 462 into repeating structures with long range order. Possibly the HOSO interacts with a  
 463 more hydrophobic cellulose plane exfoliated during the dissolution in BmimAc,  
 464 resulting in it not being completely removed during regeneration and washing. It is  
 465 also expected that H-bonding between the ester carbonyl groups in the HOSO and  
 466 the hydroxyl cellulose groups ( $\text{C}=\text{O}\cdots\text{H}$ ) is present, reinforcing the hydrophobic  
 467 interaction (Ghosh, Tran, & Rousseau, 2011). HOSO bound to cellulose would inhibit  
 468 any regular reformation of intra- and intermolecular cellulose-cellulose H-bonds, as  
 469 well as hydrophobic contacts between chains, during coagulation. Of course, the  
 470 SEM is not able to confirm any specific location of such interactions at the  
 471 magnification employed.



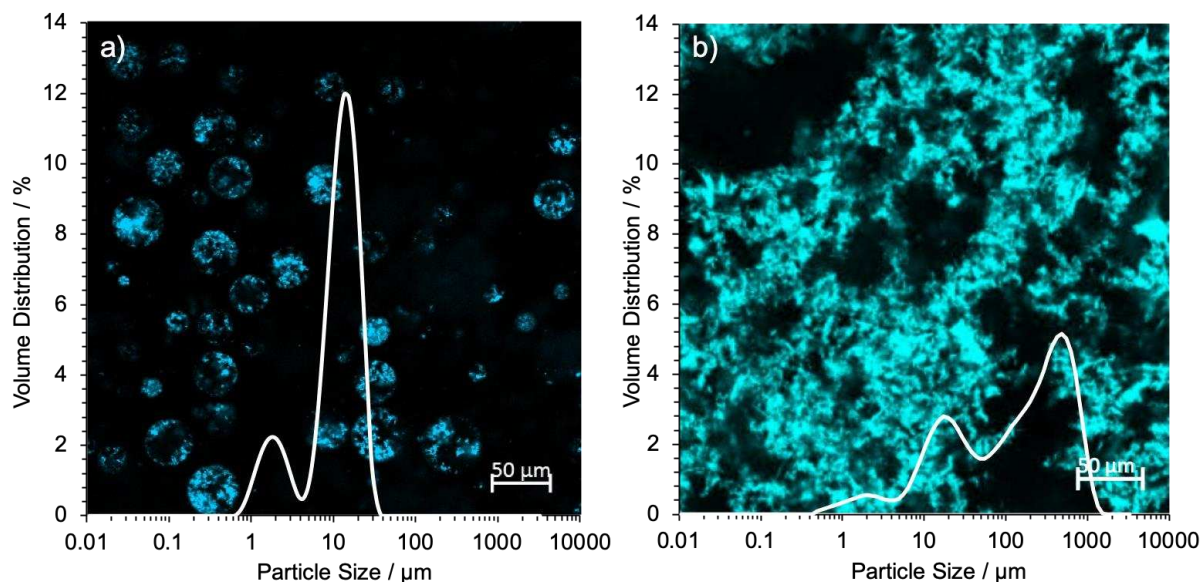
472  
 473 Fig. 3. WAXS spectra for a) cellulose powder; b) regenerated macrogel. Cellulose powder  
 474 has been fitted to Cellulose I crystal planes  $(1\bar{1}0)$ ,  $(110)$ ,  $(200)$  and amorphous cellulose  
 475 (red, green, light blue and orange peaks respectively)



476  
477 Fig. 4. SEM images of freeze-dried macrogel a) before and b) after washing in hexane. Oil  
478 droplets are seen bound to the cellulose surface in black, scale bar = 100 μm  
479

### 480 3.3 Dispersions of Oil-CMGs in water and in oil

481 In characterizing the behaviour of any new particulate emulsion stabilizer (i.e.,  
482 Pickering emulsifier) it is important to demonstrate the extent to which the particles  
483 are fully dispersed in the continuous phase, otherwise the particles are likely only to  
484 provide network stabilization via their aggregation in the bulk phase. Therefore, the  
485 regenerated oily macrogel was dispersed as far as possible in both water and HOSO  
486 separately, (Fig. 5a and b respectively). Over the range of measured cellulose  
487 concentrations (0.01 to 1.0 wt.%), oil-CMGs showed a smaller mean particle size in  
488 the oil dispersions (“oil-CMG-HOSO dispersions”) compared to the water dispersions  
489 (“oil-CM G-water dispersions”), suggesting that



490

Average Size / μm	a) 0.4 wt.% HOSO	b) 0.4 wt.% water
$(d_{3,2})$	5.98	16.8
$(d_{4,3})$	12.4	255

491 Fig. 5. Confocal images of 0.4 wt.% oil-CMGs dispersed in a) HOSO; b) water separately,  
492 with particle size data overlaid (volume distribution vs. particle size). Mean particle sizes are  
493 given in the table below. Scale bar = 50 μm

494  
 495 the regenerated cellulose is more easy to disperse in oil and therefore more  
 496 hydrophobic in character. Large aggregates were formed in water at all  
 497 concentrations, which did not break down upon further homogenisation. A mono- or  
 498 bimodal distribution of particle sizes was seen for almost all oil-CMG-HOSO  
 499 dispersions, whilst a bi- or trimodal distribution was seen for oil-CMG-water  
 500 dispersions (Fig. A3). During dispersion, formation of the interface will be fast  
 501 compared to the rate of any microgel particle absorption (Matsumiya & Murray,  
 502 2016) and it can be assumed that the gel character of the macrogel and CMGs is  
 503 similar (Murray, 2019a). The macrogels thus retain a much larger amount of water  
 504 compared to HOSO during regeneration.

505  
 506 Oily cellulose macrogels were freeze-dried, in order to remove water and to try and  
 507 determine an approximate percentage composition (see Table 1). The remaining  
 508 weight of the dried macrogel could not be entirely accounted for by cellulose alone,  
 509 considering the amount initially dissolved in the IL. Therefore, a small amount HOSO  
 510 is expected to be present in the oil-CMGs, as well as traces of IL (assuming that both  
 511 HOSO and BmimAc are not removed during freeze-drying). This was observed using  
 512 SEM (Fig. A4).

513 Table 1. Weights of oily cellulose macrogels before and after freeze-drying. The percentage  
 514 amounts of water and oil/BmimAc were calculated assuming that only water is removed  
 515 during freeze-drying

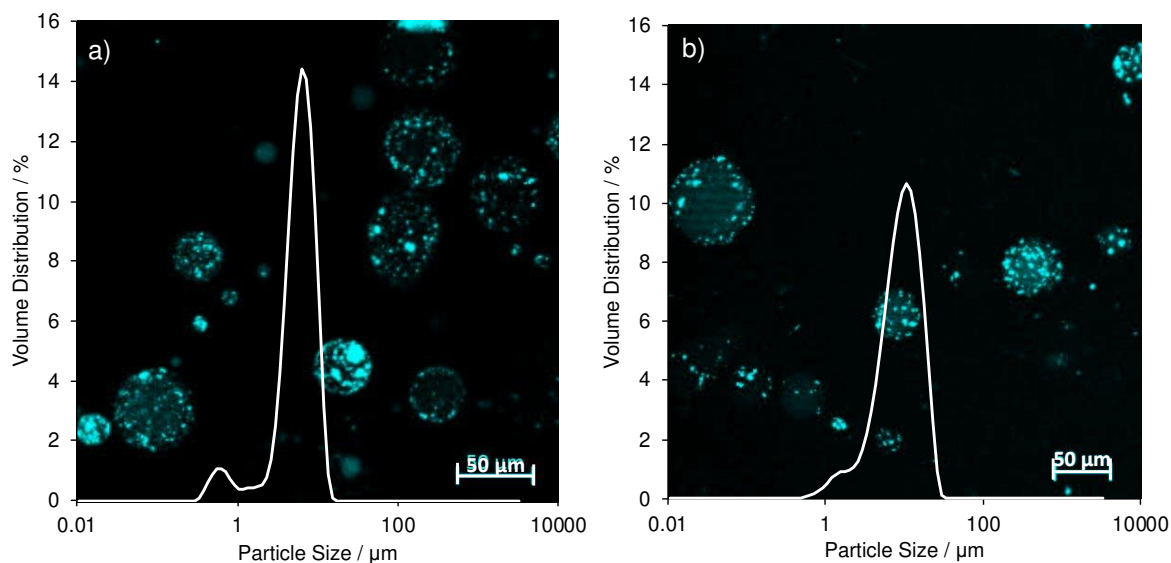
<b>Weight before drying / mg</b>	<b>Weight after drying / mg</b>	<b>Amount of water / %</b>	<b>Amount of cellulose in BmimAc / %</b>	<b>Amount of HOSO/BmimAc / %</b>
69.0	11.7	83.0	4.00	13.0
143	19.6	86.3	2.00	11.7

516 A significant amount of aggregated cellulose is also visible at the W/O interface, as  
 517 confirmed via confocal microscopy (Fig. 5a). Some microgel particles remain as  
 518 individual networks of water without attachment to water droplets, accounting for the  
 519 smaller of the two peaks seen for the particle size dispersions (1-4  $\mu\text{m}$ ) (Sarkar et  
 520 al., 2016). In oil-CMG-water dispersions, aggregation occurs and a cellulose network  
 521 forms, in order to minimise contact of the hydrophobic regions with water. Two or  
 522 three peaks are seen in the particle size dispersion (Fig. 5b), corresponding to  
 523 individual CMGs (1-4  $\mu\text{m}$ ); aggregated CMGs (10-30  $\mu\text{m}$ ) and aggregated cellulose  
 524 networks (>100  $\mu\text{m}$ ).

525 In summary, the oily macrogel is easier to break down and disperse in oil, as  
 526 expected for a suitable W/O emulsifier. However, at concentrations above ca. 1.0  
 527 wt.%, oil-CMGs were poorly dispersed in both water and HOSO: a large volume-  
 528 weighted particle size is seen for all dispersions above this concentration (Fig. A5).

529  
 530 *3.4 Water-in-oil emulsions*

531  
 532 W/O emulsions formed from both oil-CMG-HOSO and oil-CMG-water dispersions  
 533 had a surprisingly similar appearance as shown by the representative images in Fig.  
 534 6 (and extra images in Fig. A6), considering the significant difference in the  
 535 appearance and behaviour of these two dispersions as discussed in section 3.2  
 536 above. For comparison, W/O emulsions formed from CMGs without the addition of  
 537 oil during regeneration gave relatively poor interfacial coverage and separated out  
 538 within a few days, most likely due to more problematic dispersion of the macrogel  
 539 (data not shown).



540

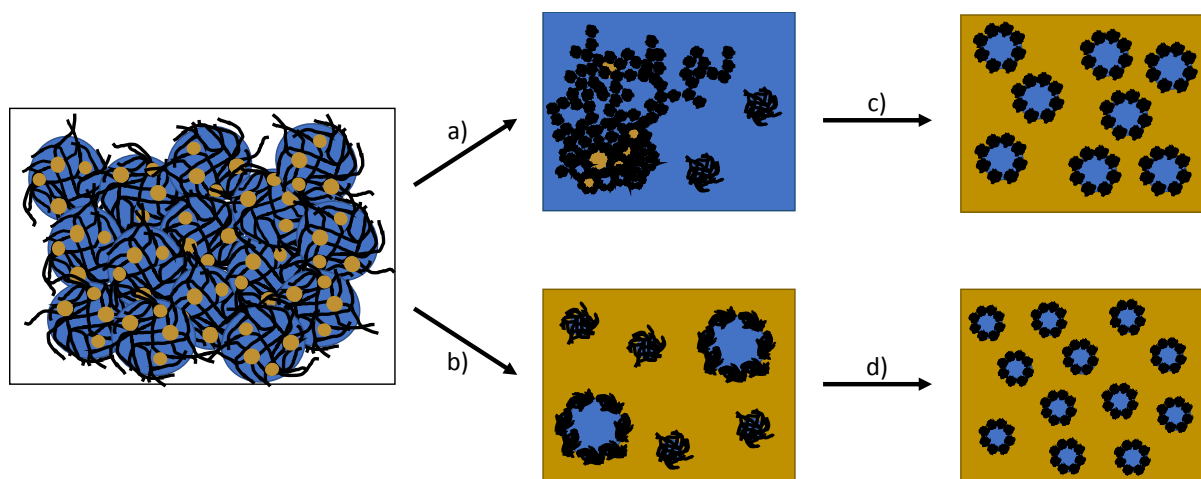
Average Size / $\mu\text{m}$	0.1 wt.% HOSO (W/O)	0.1 wt.% water (W/O)
$(d_{3,2})$	3.74	3.90
$(d_{4,3})$	6.10	6.28

541 Fig. 6. Confocal images of 10 vol.% W/O emulsions formed from 0.1 wt.% oil-CMG-HOSO a)  
 542 oil-CMG-HOSO oil dispersion; b) CMG-water dispersion, with particle size data overlaid  
 543 (volume distribution vs. particle size). Mean particle sizes are given in the table below. Scale  
 544 bar = 50  $\mu\text{m}$

545 In addition, the PSDs of the emulsions were also approximately the same,  
 546 regardless of the dispersion route. This was observed for W/O emulsions made from  
 547 oil-CMG-water and oil-CMG-HOSO dispersions over a range of concentrations (Fig.  
 548 A7). At the lowest CMG concentrations (ca. 0.05 wt.%) some droplet flocculation was  
 549 observed, whilst at the highest CMG concentrations (>5 wt.%), droplet size  
 550 increased (Fig. A7a-c). The average particle size was generally marginally smaller  
 551 for W/O emulsions formed from the oil-CMG-HOSO dispersions, possibly owing to  
 552 the initial smaller size of CMGs in the dispersions. These results confirm a) the  
 553 amphiphilic nature of the oil-CMGs; b) the 'limiting factor' for droplet size, as  
 554 discussed below.

555 Fig. 7 shows a possible schematic describing the dispersion and emulsification  
 556 stages, discussed as follows. Firstly, the PSD reduces upon emulsification and the

557 resultant increased area of the water-oil interface. For oil-CMG-HOSO dispersions,  
 558 the addition of extra water during the formation of the final W/O emulsions breaks  
 559 down aggregates of cellulose at the water-oil interface, since there is a larger  
 560 boundary area available to which CMGs can adsorb. Therefore, the average CMG  
 561 particle size reduces and smaller water droplets can be stabilised (Fig. 6a). Droplets  
 562 are further broken down by more passes through the homogeniser, owing to higher  
 563 energy input and resultant increase in disruption (due to turbulence and cavitation)  
 564 (Long, Zhao, Zhao, Yang, & Liu, 2012). The CMGs eventually form a more uniform  
 565 layer around the final W/O droplets and a relatively monodisperse droplet size is  
 566 recorded (see Fig. 6a). A similar situation arises when oil-CMG-water dispersions  
 567 are homogenised with extra added oil, since the extent of the available W/O interface  
 568 becomes identical. Homogenisation helps to break up cellulose networks and fast  
 569 absorption of CMGs to the water-oil interface prevents CMG re-aggregation (e.g.,  
 570 see Fig. 6b). Consequently, the appearance and the PSD of the final W/O emulsions  
 571 are very similar. Very few free (i.e. non-adsorbed) CMGs are observable in the  
 572 emulsions, confirming their amphiphilicity.

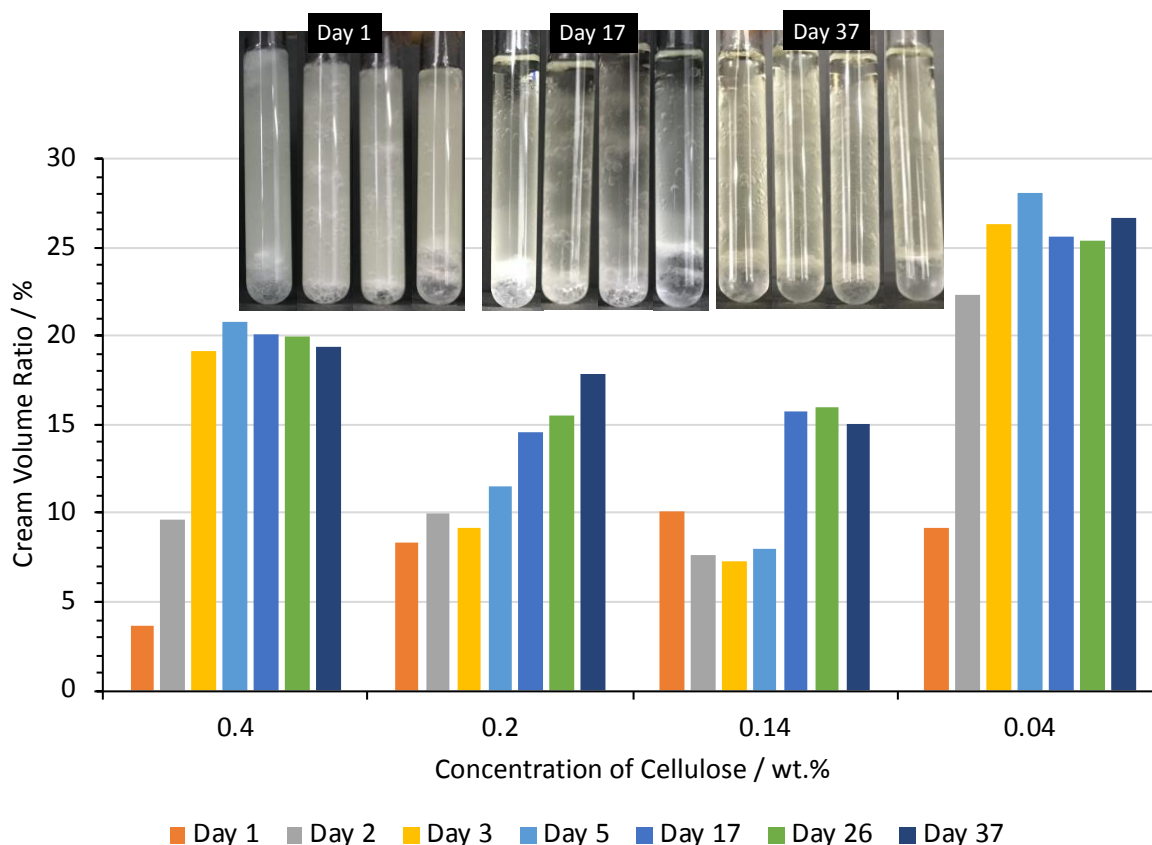


573  
 574 Fig. 7. Schematic showing dispersion and emulsification of oil-CMGs, from left to right: initial  
 575 cellulose macrogel; a) oil-CMG-water dispersion; b) oil-CMG-oil dispersion; c and d)  
 576 emulsification to form oil-CMG-stabilised W/O emulsion (from oil-CMG-water and oil-CMG-  
 577 HOSO dispersions, respectively). Water is shown in blue, oil in yellow and cellulose in black

578 Secondly, it would appear that the emulsification method is the limiting factor for  
 579 droplet size distribution - since droplet size is fairly uniform, regardless of the  
 580 dispersion route (see confocal images, Fig. 6 and Fig. A6). In this case, the oil, water  
 581 and CMG amounts are consistent and therefore the emulsions formed are almost  
 582 identical. Increasing the water content to 20 vol.% gave similar droplets sizes to 10  
 583 vol.% water emulsions, with droplets remaining uniform in size across a range of  
 584 cellulose concentrations (Fig. A8). This suggests that for concentrations within the  
 585 range 0.05 to 0.25 wt.% CMG, the CMG emulsifier is present in excess and the  
 586 droplet size depends primarily on the homogenisation conditions (McClements,  
 587 2004).

588  
 589 *3.5 W/O emulsion stability tests*

590  
591 The stability of the W/O emulsions formed via both routes was monitored by  
592 measuring the cream volume ratio. PSD measurements, light and confocal  
593 microscopy as a function of storage time. W/O emulsions from both oil-CMG-HOSO  
594 and oil-CMG-water dispersions exhibited similar creaming behaviour, (data not  
595 shown). Fig. 8 gives the change in cream volume over a period of 37 days, with  
596 images shown in the inset, for 20 vol.% W/O emulsions from oil-CMG-water  
597 dispersions. Four concentrations are given: 0.04, 0.14, 0.2 and 0.4 wt.% cellulose.  
598 The cream volume ratio did not reach the internal phase volume percentage (20  
599 vol.%) for emulsions made with 0.14 and 0.2 wt.% oil-CMG, demonstrating that  
600 some water remained in the emulsion over the period of time measured. No phase  
601 inversion occurred over the 37-day period and a stable emulsion volume in the tube  
602 was observable from day 17, for 0.14 wt.% cellulose. Oil-CMG-stabilised water  
603 droplets were still clearly visible in the emulsions after 7 days via light and confocal  
604 microscopy (Fig. A9), with no significant change in droplet size. The increase in  
605 cream volume ratio over the period of observation is most likely due to larger water  
606 droplets sedimenting out. This was confirmed by size measurements: emulsions  
607 were sampled from the top emulsion layer only and average PSDs shifted to smaller  
608 values over time. Larger droplets appear to settle out over time and smaller droplets  
609 remain well-stabilised in the emulsion (Fig. A10). When the emulsion was shaken  
610 and sampled after storage, a large mean droplet size was recorded, due to the re-  
611 incorporation of the lower layer and therefore larger droplets (Fig. A11). Through  
612 further homogenisation steps, it may be possible to increase the uniformity of the  
613 droplet size distribution and improve the overall stability of the emulsion, preventing  
614 noticeable sedimentation.

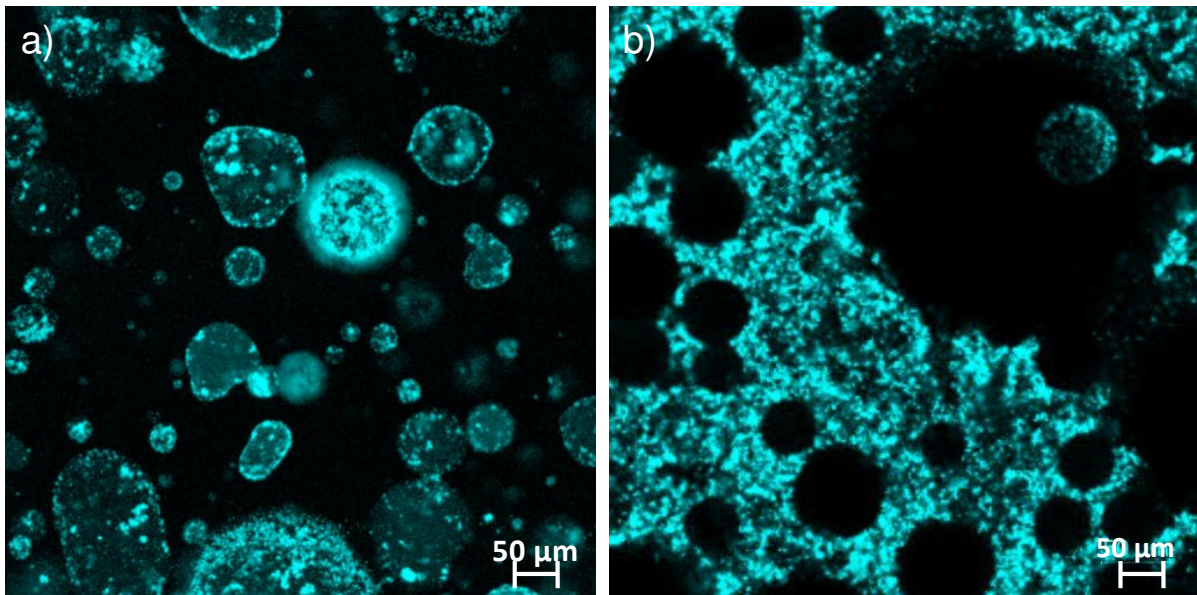


615  
616 Fig. 8. Cream Volume Ratio heights over 37 days for 20 vol.% W/O emulsions formed from  
617 0.4, 0.2, 0.14 and 0.04 wt.% oil-CMG-HOSO dispersions. Inset: pictures of emulsions from  
618 left to right on day 1, day 17 and day 37 (from left to right: 0.4, 0.2, 0.14 and 0.04 wt.%)

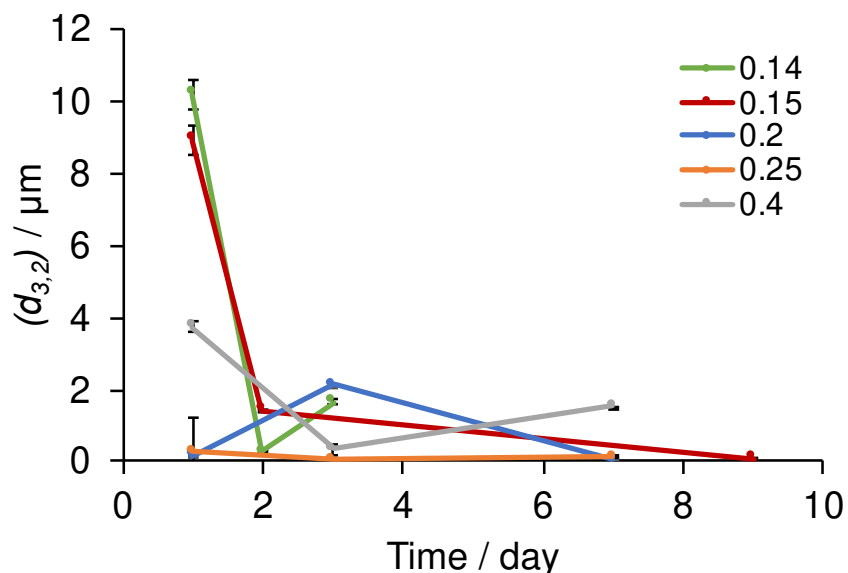
619 Evidently, a delicate balance between CMG and internal phase amount is required to  
620 produce W/O emulsions of good stability. From the cream volume ratio data, a  
621 concentration of ca. 0.2 wt.% cellulose seems to be the optimum. Sufficient oil-CMG  
622 must be added in order to cover the water-oil interface and provide good coverage,  
623 however addition of excess oil-CMG leads to seemingly irreversible aggregation of  
624 cellulose in the continuous oil phase. This was evidenced in the confocal images  
625 (Fig. 9). Good cellulose coverage is visible for an emulsion of 0.2 wt.% cellulose,  
626 with Pickering-type stabilization via oil-CMGs and non-spherical droplets. However,  
627 an aggregated network of flocculated oil-CMGs is visible in the continuous phase at  
628 0.4 wt.% cellulose, stabilising larger water droplets.

629 Such behaviour was confirmed by particle size measurements, where size over time  
630 is quantified by ( $d_{3,2}$ ) values of the emulsions, at various concentrations of oil-CMG  
631 (Fig. 10). The highest emulsion stability was observed for 0.2 to 0.25 wt.% cellulose,  
632 which gave the smallest initial droplet sizes and values remaining within a 2  $\mu\text{m}$   
633 range during 1 week of storage. For concentrations <0.25 wt.% cellulose, the initial  
634 particle size was relatively large due to insufficient droplet coverage but decreased  
635 over time, most probably due to sedimentation of larger droplets, (as discussed  
636 above). For concentrations >0.25 wt.%, the initial droplet size increased again  
637 relative to 0.25 wt.%, possibly due to the presence of excess, flocculated oil-CMGs  
638 in the oil phase. However, over time particle size became comparable to 0.2 to 0.25

639 wt.% cellulose emulsions with no significant sedimentation observable. Confocal  
 640 images show that at larger concentrations, oil-CMGs adsorb to the interface over  
 641 time, leading to better coverage of water droplets and higher stability (Fig. A12).  
 642 Therefore, although higher concentrations of cellulose may lead to an initially larger  
 643 particle size, rearrangement of oil-CMGs at the interface allows space for excess  
 644 CMG in the oil phase to spontaneously adsorb to the interface. “De-flocculation” may  
 645 occur, due to the rearrangement of the polymer chains within the oil-CMGs, resulting  
 646 in a particle size reduction. This behaviour has also been reported for poly(*N*-  
 647 isopropylacrylamide) (pNIPAM) polymer microgels (Pinaud et al., 2014).



648  
 649 Fig. 9. Confocal images of 20 vol.% W/O emulsions stabilised by a) 0.2 wt.% oil-CMG; b) 0.4  
 650 wt.% oil-CMG. Scale bar = 50 μm



651  
 652 Fig. 10. Changes in the particle size of W/O emulsions over time, with 0.14, 0.15, 0.2, 0.25  
 653 and 0.4 wt.% oil-CMG-emulsifier (green, red, blue, orange and grey respectively). Particle  
 654 size is given as the surface-weighted mean diameter ( $d_{3,2}$ )

655 It is also important to consider the amount of cellulose present during regeneration,  
656 i.e. the amount of cellulose dissolved initially in the IL, which also affects the size and  
657 packing of the cellulose networks in the CMGs. A denser gel network is expected to  
658 form at higher wt.% cellulose in the IL, potentially increasing the adsorption and  
659 retention of oil during the regeneration process. However, higher density may lead to  
660 reduced macrogel break down, yielding a greater average CMG particle size and a  
661 larger overall droplet size in the final emulsion. Furthermore, it has been reported  
662 that microgels with lower cross-link densities display faster adsorption rates to the  
663 interface and higher compressibility. A more elastic interface is expected to give  
664 higher stability (Pinaud et al., 2014). The effect of network density on emulsion  
665 stability is currently being investigated, alongside studies employing NMR and FTIR  
666 in order to further understand the mechanism of CMG-regeneration. Such  
667 investigations aim to probe the interactions between cellulose and oil, as well as  
668 each of their individual interactions with 1-butanol and the IL during regeneration.  
669

#### 670 **4. Conclusions**

671 A natural, unmodified cellulose emulsifier has been prepared, by fabricating a  
672 “hydrophobic” microgel using a facile regeneration method from an IL. An edible oil  
673 was introduced to the cellulose after dissolution, which appeared to remain bound in  
674 some way to the cellulose throughout the coagulation process, as confirmed using  
675 FTIR, SEM and WAXS. It is suggested that an “oily” or hydrophobic surface is  
676 exposed, allowing the cellulose to act as a W/O emulsifier after breakdown to form  
677 microgel particles in a dispersion. The oily macrogel was much easier to disperse in  
678 oil and a better W/O emulsifier – W/O emulsions containing 0.2 wt.% cellulose and at  
679 least 20 vol.% water being stable for at least 4 weeks. At higher concentrations, an  
680 increase in CMG present in the continuous phase resulted in formation of flocculated  
681 microgel regions. Regeneration from higher wt.% cellulose/IL solutions is thought to  
682 increase the density of the cellulose gel network, possibly leading to a higher  
683 retention of oil and resulting in even better CMG-W/O surface activity, whilst also  
684 affecting their swelling properties at the interface (Pinaud et al., 2014).

685 Thus, the current study proposes a novel approach to forming a hydrophobic  
686 cellulose-based emulsifier without employing chemical modification, that meets the  
687 demand for a natural, renewable W/O emulsifier. This could be of great value to the  
688 food industry as a method of reducing fat as well as finding applications in  
689 agricultural, cosmetic and medical areas. Further work on the understanding of the  
690 interactions between the cellulose and the oil in both the microgels and the  
691 emulsions is required to optimise the W/O emulsion formulations. Shelf-stability of  
692 the CMGs as ingredients could also be addressed by considering their dried and  
693 swollen states.

694

#### 695 **Acknowledgements**

696 The authors gratefully acknowledge the Engineering and Physical Sciences  
 697 Research Council (EPSRC) funded Centre for Doctoral Training in Soft Matter and  
 698 Functional Interfaces (SOFI), Grant Ref. No. EP/L015536/1 as well as Mondelēz  
 699 International (Reading, UK) for financial support. Access to the Zeiss LSM700  
 700 microscope was provided by the Bioimaging Facility of the Faculty of Biological  
 701 Sciences of the University of Leeds. We also wish to thank Andrew Hobson and  
 702 Alexander Kulak (both University of Leeds) for their help and assistance with the  
 703 FTIR and SEM, respectively and finally, Aurimas Šeimys for his initial work on the  
 704 project.

## 705 706 **References**

- 707  
 708 Albert, C., Beladjine, M., Tsapis, N., Fattal, E., Agnely, F., & Huang, N. (2019). Pickering emulsions:  
 709 Preparation processes, key parameters governing their properties and potential for  
 710 pharmaceutical applications. *Journal of Controlled Release*, *309*(July), 302–332.  
 711 <https://doi.org/10.1016/j.jconrel.2019.07.003>  
 712 Arditty, S., Whitby, C. P., Binks, B. P., Schmitt, V., & Leal-Calderon, F. (2003). Some general features  
 713 of limited coalescence in solid-stabilized emulsions. *European Physical Journal E*, *11*(3), 273–  
 714 281. <https://doi.org/10.1140/epje/i2003-10018-6>  
 715 Azmi, N. A. N., Elgharbawy, A. A. M., Motlagh, S. R., Samsudin, N., & Salleh, H. M. (2019).  
 716 Nanoemulsions: Factory for food, pharmaceutical and cosmetics. *Processes*, *7*(9).  
 717 <https://doi.org/10.3390/pr7090617>  
 718 Bastida-Rodríguez, J. (2013). The Food Additive Polyglycerol Polyricinoleate (E-476): Structure,  
 719 Applications, and Production Methods. *ISRN Chemical Engineering*, *2013*, 1–21.  
 720 <https://doi.org/10.1155/2013/124767>  
 721 Bertsch, P., Arcari, M., Geue, T., Mezzenga, R., Nyström, G., & Fischer, P. (2019). Designing  
 722 Cellulose Nanofibrils for Stabilization of Fluid Interfaces. *Biomacromolecules*, *20*(12), 4574–  
 723 4580. <https://doi.org/10.1021/acs.biomac.9b01384>  
 724 Borreani, J., Hernando, I., & Quiles, A. (2020). Cream replacement by hydrocolloid-stabilized  
 725 emulsions to reduce fat digestion in panna cottas. *Lwt*, *119*(November 2019), 108896.  
 726 <https://doi.org/10.1016/j.lwt.2019.108896>  
 727 Burgaud, I., Dickinson, E., & Nelson, P. V. (1990). An improved high-pressure homogenizer for  
 728 making fine emulsions on a small scale. *International Journal of Food Science & Technology*,  
 729 *25*(1), 39–46. <https://doi.org/10.1111/j.1365-2621.1990.tb01057.x>  
 730 Cai, J., & Zhang, L. (2005). Rapid dissolution of cellulose in LiOH/urea and NaOH/urea aqueous  
 731 solutions. *Macromolecular Bioscience*, *5*(6), 539–548. <https://doi.org/10.1002/mabi.200400222>  
 732 Chua, E. T., Brunner, M., Atkin, R., Eltanahy, E., Thomas-Hall, S. R., & Schenk, P. M. (2019). The  
 733 Ionic Liquid Cholinium Arginate Is an Efficient Solvent for Extracting High-Value  
 734 Nannochloropsis sp. Lipids. *ACS Sustainable Chemistry and Engineering*, *7*(2), 2538–2544.  
 735 <https://doi.org/10.1021/acssuschemeng.8b05448>  
 736 Dickinson, E. (2011). Double Emulsions Stabilized by Food Biopolymers. *Food Biophysics*, *6*(1), 1–  
 737 11. <https://doi.org/10.1007/s11483-010-9188-6>  
 738 Dickinson, E. (2012). Use of nanoparticles and microparticles in the formation and stabilization of food  
 739 emulsions. *Trends in Food Science and Technology*, *24*(1), 4–12.  
 740 <https://doi.org/10.1016/j.tifs.2011.09.006>  
 741 Fan, Z., Chen, J., Guo, W., Ma, F., Sun, S., & Zhou, Q. (2018). Anti-solvents tuning cellulose  
 742 nanoparticles through two competitive regeneration routes. *Cellulose*, *25*(8), 4513–4523.  
 743 <https://doi.org/10.1007/s10570-018-1897-x>  
 744 Fink, H. P., Weigel, P., Purz, H. J., & Ganster, J. (2001). Structure formation of regenerated cellulose  
 745 materials from NMMO-solutions. *Progress in Polymer Science (Oxford)*, *26*(9), 1473–1524.  
 746 [https://doi.org/10.1016/S0079-6700\(01\)00025-9](https://doi.org/10.1016/S0079-6700(01)00025-9)  
 747 Fryczkowska, B., Kowalska, M., Biniias, D., Slusarczyk, C., Janicki, J., Sarna, E., & Wyszomirski, M.  
 748 (2018). Properties and Structure of Cellulosic Membranes Obtained from Solutions in Ionic  
 749 Liquids Coagulated in Primary Alcohols. *Autex Research Journal*, *18*(3), 232–242.  
 750 <https://doi.org/10.1515/aut-2017-0036>  
 751 Ghosh, S., & Rousseau, D. (2011). Fat crystals and water-in-oil emulsion stability. *Current Opinion in*

- 752 *Colloid and Interface Science*, 16(5), 421–431. <https://doi.org/10.1016/j.cocis.2011.06.006>
- 753 Ghosh, S., Tran, T., & Rousseau, D. (2011). Comparison of pickering and network stabilization in  
754 water-in-oil emulsions. *Langmuir*, 27(11), 6589–6597. <https://doi.org/10.1021/la200065y>
- 755 Gómez, M., & Martínez, M. M. (2018). Fruit and vegetable by-products as novel ingredients to  
756 improve the nutritional quality of baked goods. *Critical Reviews in Food Science and Nutrition*,  
757 58(13), 2119–2135. <https://doi.org/10.1080/10408398.2017.1305946>
- 758 Gupta, K. M., Hu, Z., & Jiang, J. (2013). Cellulose regeneration from a cellulose/ionic liquid mixture:  
759 The role of anti-solvents. *RSC Advances*, 3(31), 12794–12801.  
760 <https://doi.org/10.1039/c3ra40807h>
- 761 Hedlund, A., Köhnke, T., Hagman, J., Olsson, U., & Theliander, H. (2019). Microstructures of  
762 cellulose coagulated in water and alcohols from 1-ethyl-3-methylimidazolium acetate:  
763 contrasting coagulation mechanisms. *Cellulose*, 26(3), 1545–1563.  
764 <https://doi.org/10.1007/s10570-018-2168-6>
- 765 Huang, S., Liu, X., Chang, C., & Wang, Y. (2020). Recent developments and prospective food-related  
766 applications of cellulose nanocrystals: a review. *Cellulose*, 27(6), 2991–3011.  
767 <https://doi.org/10.1007/s10570-020-02984-3>
- 768 Kopelman, P. G. (2000). Obesity as a medical problem. *Nature*. <https://doi.org/10.1038/35007508>
- 769 Long, Z., Zhao, M., Zhao, Q., Yang, B., & Liu, L. (2012). Effect of homogenisation and storage time on  
770 surface and rheology properties of whipping cream. *Food Chemistry*, 131(3), 748–753.  
771 <https://doi.org/10.1016/j.foodchem.2011.09.028>
- 772 Marchetti, L., Muzzio, B., Cerrutti, P., Andrés, S. C., & Califano, A. N. (2017). Bacterial nanocellulose  
773 as novel additive in low-lipid low-sodium meat sausages. Effect on quality and stability. *Food*  
774 *Structure*, 14(June), 52–59. <https://doi.org/10.1016/j.foostr.2017.06.004>
- 775 Martínez, R. M., Rosado, C., Velasco, M. V. R., Lannes, S. C. S., & Baby, A. R. (2019). Main features  
776 and applications of organogels in cosmetics. *International Journal of Cosmetic Science*, 41(2),  
777 109–117. <https://doi.org/10.1111/ics.12519>
- 778 Matsumiya, K., & Murray, B. S. (2016). Soybean protein isolate gel particles as foaming and  
779 emulsifying agents. *Food Hydrocolloids*, 60, 206–215.  
780 <https://doi.org/10.1016/j.foodhyd.2016.03.028>
- 781 McClements, D. J. (2004). *Food Emulsion Principle, Practices, and Techniques*. Retrieved from  
782 [https://diglib.mrgums.ac.ir/Uploads/User/4375/کتابخانه/D.\\_J.\\_McClements-](https://diglib.mrgums.ac.ir/Uploads/User/4375/کتابخانه/D._J._McClements-Food_emulsions_principles_practices_and_techniques-CRC_Press(2005).pdf)  
783 [Food\\_emulsions\\_principles\\_practices\\_and\\_techniques-CRC\\_Press\(2005\).pdf](https://diglib.mrgums.ac.ir/Uploads/User/4375/کتابخانه/D._J._McClements-Food_emulsions_principles_practices_and_techniques-CRC_Press(2005).pdf)
- 784 Mitsou, E., Tavantzis, G., Sotiroidis, G., Ladikos, D., Xenakis, A., & Papadimitriou, V. (2016). Food  
785 grade water-in-oil microemulsions as replacement of oil phase to help process and stabilization  
786 of whipped cream. *Colloids and Surfaces A: Physicochemical and Engineering Aspects*, 510,  
787 69–76. <https://doi.org/10.1016/j.colsurfa.2016.07.001>
- 788 Mortensen, A., Aguilar, F., Crebelli, R., Di Domenico, A., Dusemund, B., Frutos, M. J., ... Lambré, C.  
789 (2017). Re-evaluation of polyglycerol polyricinoleate (E 476) as a food additive. *EFSA Journal*,  
790 15(3). <https://doi.org/10.2903/j.efsa.2017.4743>
- 791 Murray, B. S. (2019a). Microgels at fluid-fluid interfaces for food and drinks. *Advances in Colloid and*  
792 *Interface Science*, 271, 101990. <https://doi.org/10.1016/j.cis.2019.101990>
- 793 Murray, B. S. (2019b). Pickering emulsions for food and drinks. *Current Opinion in Food Science*, 27,  
794 57–63. <https://doi.org/10.1016/j.cofs.2019.05.004>
- 795 Neethirajan, S., Kobayashi, I., Nakajima, M., Wu, D., Nandagopal, S., & Lin, F. (2011). Microfluidics  
796 for food, agriculture and biosystems industries. *Lab on a Chip*, 11(9), 1574–1586.  
797 <https://doi.org/10.1039/c0lc00230e>
- 798 Oh, S. Y., Yoo, D. I., Shin, Y., & Seo, G. (2005). FTIR analysis of cellulose treated with sodium  
799 hydroxide and carbon dioxide. *Carbohydrate Research*, 340(3), 417–428.  
800 <https://doi.org/10.1016/j.carres.2004.11.027>
- 801 Ossowicz, P., Kleboko, J., Roman, B., Janus, E., & Rozwadowski, Z. (2019). The relationship  
802 between the structure and properties of amino acid ionic liquids. *Molecules*, 24(18).  
803 <https://doi.org/10.3390/molecules24183252>
- 804 Ozturk, B., & McClements, D. J. (2016). Progress in natural emulsifiers for utilization in food  
805 emulsions. *Current Opinion in Food Science*, 7, 1–6. <https://doi.org/10.1016/j.cofs.2015.07.008>
- 806 Pang, M., Huang, Y., Meng, F., Zhuang, Y., Liu, H., Du, M., ... Cai, Y. (2020). Application of bacterial  
807 cellulose in skin and bone tissue engineering. *European Polymer Journal*, 122(November 2019),  
808 109365. <https://doi.org/10.1016/j.eurpolymj.2019.109365>
- 809 Paunonen, S., Kamppuri, T., Katajainen, L., Hohenthal, C., Heikkilä, P., & Harlin, A. (2019).  
810 Environmental impact of cellulose carbamate fibers from chemically recycled cotton. *Journal of*  
811 *Cleaner Production*, 222, 871–881. <https://doi.org/10.1016/j.jclepro.2019.03.063>

- 812 Pinaud, F., Geisel, K., Massé, P., Catargi, B., Isa, L., Richtering, W., ... Schmitt, V. (2014). Adsorption  
813 of microgels at an oil-water interface: Correlation between packing and 2D elasticity. *Soft Matter*,  
814 *10*(36), 6963–6974. <https://doi.org/10.1039/c4sm00562g>
- 815 Qi, H., Yang, Q., Zhang, L., Liebert, T., & Heinze, T. (2011). The dissolution of cellulose in NaOH-  
816 based aqueous system by two-step process. *Cellulose*, *18*(2), 237–245.  
817 <https://doi.org/10.1007/s10570-010-9477-8>
- 818 Rogers, M. A., Wright, A. J., & Marangoni, A. G. (2009). Oil organogels: The fat of the future? *Soft*  
819 *Matter*, *5*(8), 1594–1596. <https://doi.org/10.1039/b822008p>
- 820 Rohman, A., & Che Man, Y. B. (2012). Quantification and classification of corn and sunflower oils as  
821 adulterants in olive oil using chemometrics and FTIR spectra. *The Scientific World Journal*,  
822 *2012*. <https://doi.org/10.1100/2012/250795>
- 823 Sadeghifar, H., Venditti, R., Pawlak, J. J., & Jur, J. (2019). Cellulose transparent and flexible films  
824 prepared from DMAc/LiCl solutions. *BioResources*, *14*(4), 9021–9032.
- 825 Sarkar, A., Murray, B., Holmes, M., Ettelaie, R., Abdalla, A., & Yang, X. (2016). In vitro digestion of  
826 Pickering emulsions stabilized by soft whey protein microgel particles: Influence of thermal  
827 treatment. *Soft Matter*, *12*(15), 3558–3569. <https://doi.org/10.1039/c5sm02998h>
- 828 Stana-Kleinschek, K., Ribitsch, V., Kreze, T., & Fras, L. (2002). Determination of the adsorption  
829 character of cellulose fibres using surface tension and surface charge. *Materials Research*  
830 *Innovations*, *6*(1), 13–18. <https://doi.org/10.1007/s10019-002-0168-4>
- 831 Sun, L., Chen, J. Y., Jiang, W., & Lynch, V. (2015). Crystalline characteristics of cellulose fiber and  
832 film regenerated from ionic liquid solution. *Carbohydrate Polymers*, *118*, 150–155.  
833 <https://doi.org/10.1016/j.carbpol.2014.11.008>
- 834 Tan, X., Chen, L., Li, X., & Xie, F. (2019). Effect of anti-solvents on the characteristics of regenerated  
835 cellulose from 1-ethyl-3-methylimidazolium acetate ionic liquid. *International Journal of Biological*  
836 *Macromolecules*, *124*, 314–320. <https://doi.org/10.1016/j.ijbiomac.2018.11.138>
- 837 Verma, C., Mishra, A., Chauhan, S., Verma, P., Srivastava, V., Quraishi, M. A., & Ebenso, E. E.  
838 (2019). Dissolution of cellulose in ionic liquids and their mixed cosolvents: A review. *Sustainable*  
839 *Chemistry and Pharmacy*, *13*(July), 100162. <https://doi.org/10.1016/j.scp.2019.100162>
- 840 Wang, Z., & Wang, Y. (2016). Tuning Amphiphilicity of Particles for Controllable Pickering Emulsion.  
841 *Materials*, *9*(11). <https://doi.org/10.3390/ma9110903>
- 842 Wilson, R., & Smith, M. (1998). Human studies on polyglycerol polyricinoleate (PGPR). *Food and*  
843 *Chemical Toxicology*, *36*(9–10), 743–745. [https://doi.org/10.1016/S0278-6915\(98\)00058-1](https://doi.org/10.1016/S0278-6915(98)00058-1)
- 844 Yan, L., & Gao, Z. (2008). Dissolving of cellulose in PEG/NaOH aqueous solution. *Cellulose*, *15*(6),  
845 789–796. <https://doi.org/10.1007/s10570-008-9233-5>
- 846 Zhang, J., Wu, J., Yu, J., Zhang, X., He, J., & Zhang, J. (2017). Application of ionic liquids for  
847 dissolving cellulose and fabricating cellulose-based materials: State of the art and future trends.  
848 *Materials Chemistry Frontiers*. Mater. Chem. Front. <https://doi.org/10.1039/c6qm00348f>  
849